

Sample Description and Locations

Agua de Dionisio extrusive samples

SR62 (27.277260°W 66.744710°S; 360 m)

Crystal-rich pumice clast (~50 % crystals) with phenocrysts of plagioclase, fine-grained biotite, amphibole and quartz.

SR59 (27.277900°W 66.737510°S; 270 m)

Pumice clast with ~ 30 % crystallinity. Phenocrysts of plagioclase, amphibole and biotite are present.

SR63 (27.278790°W 66.739110°S; 250 m)

Pumice clast containing ~35 % crystals. Phenocrysts of plagioclase, biotite and amphibole are present.

SR73 (27.279782°W 66.737823°S; 220 m)

Relatively crystal-poor pumice clast containing ~25 % crystals dominated by plagioclase, biotite and amphibole, with the remainder made up of microlithic devitrified glass.

SR65 (27.279350°W 66.734550°S; 130 m)

Dacitic pumice clast containing ~40 % crystals. Plagioclase, biotite and amphibole are the major phenocryst phases.

SR43 (27.279945°W 66.729370°S; 45 m)

Strongly altered pumice from the base of the Agua de Dionisio section. Original texture is replaced by secondary carbonate and chlorites. Relicts of plagioclase, biotite and amphibole are present.

Intrusive Samples from the FNVC

YB42 (*Farallón Negro Mine, Esparansa SE level 2517, Tope 2, in the Transport gallery*)

A quartz-feldspar porphyry that intruded the Alto de la Blenda stock. For location on a map refer to Márquez Zavalía and Heinrich (2016). It is cross-cut by a late carbonate vein. This sample exhibits strong feldspar destructive alteration.

P4 (27.326291°W 66.607599°S; *Bajo de la Alumbreira Open Pit*)

This porphyry intrusion is a post-mineralization dike from the Bajo de la Alumbreira mine, which cross-cuts the two main mineralization events. This sample has a porphyritic texture and contains phenocrysts of plagioclase, amphibole, biotite and quartz.

P2 (27.329730°W 66.607487°S; *Bajo de la Alumbreira Open Pit*)

This is the earliest porphyry intrusion in the Bajo de la Alumbreira porphyry copper deposit. It hosts strong quartz-magnetite alteration with abundant quartz veins. All of the Cu mineralization either comes together with or post-dates this intrusion.

Analytical Methods

Zircon trace element analyses and U-Pb geochronology

Zircon grains of each sample were loaded into quartz crucibles and annealed in a high temperature furnace (900 °C) before they were mounted in epoxy resin, polished to their centres, carbon coated and imaged by cathodoluminescence (CL).

Selected zircon grains (Fig. DR1) were analyzed for in-situ trace element concentrations by laser ablation-inductively coupled plasma-mass spectrometry (LA-ICP-MS) using a 193 nm Resonetics ArF excimer laser coupled to a Thermo Element XR ICP-MS at the Institute of Geochemistry and Petrology, ETH Zurich. The output energy of the laser was typically $\sim 2 \text{ J/cm}^2$ and used a 5 Hz pulse repetition rate with a crater size of 30 μm . Routine measurements of NIST 610 silicate glass (twice every 25 zircon analyses) were used as external standards to correct for instrumental drift. The ablation locations were selected based on CL images and a spot size of 30 μm was used (Fig. DR1). Dwell times ranged from 5 - 30 ms and peak-hopping was employed. Oxide generation was optimised at $\text{ThO}^+/\text{Th}^+ = <0.2\%$. For each analysis a baseline of 30 seconds was measured and prior to 40 seconds of ablation. Elemental concentrations were obtained using Iolite (Paton et al., 2011) using the zircon stoichiometric SiO_2 concentration of 32.8 wt % as an internal standard. The accuracy of the measurements was monitored by repeated analyses of secondary zircon standards (GJ-1 and 91500). Zircons showing clear inheritance and analyses with anomalously high Al, P, Ba, La (indicating the presence of mineral/melt inclusions) are excluded from the reported data. Typical uncertainty of the element concentration is in the range of 5% for elements well above the limit of detection (LOD) and larger for concentrations closer to the LOD.

After LA-ICP-MS analyses selected zircon grains were extracted from the grain mount and transferred to 3 ml Savillex PFA Hex beakers, rinsed with 3 N HNO_3 and loaded into 200 μl Savillex microcapsules with concentrated HF + trace HNO_3 and chemically abraded at 180 °C for 12–15 hours (Mattinson, 2005). The zircons were transferred back into the 3 ml for cleaning with 3 N HNO_3 and 6 N HCl before reloading into their respective 200 μl Savillex microcapsules, where they were spiked using the EARTHTIME ^{202}Pb - ^{205}Pb - ^{233}U - ^{235}U tracer solution (ET2535; Condon et al., 2015; McLean

et al., 2015) and dissolved in concentrated HF and trace HNO₃ for approximately 60 hours. The samples were dried down and redissolved in 6N HCl at 180 °C for 12 hours to convert the samples to chlorides. The solutions were dried again and redissolved in 3N HCl. Uranium and Pb were then separated using ion exchange chromatography following procedures modified after Krogh (1973). Both U and Pb were loaded together onto zone-refined single Re filaments with one microdrop of a silica gel emitter (Gerstenberger and Haase, 1997). All measurements were performed at ETH Zurich on a Thermo-Scientific TRITONPLUS thermal ionisation mass spectrometer (TIMS). Pb was measured sequentially on a dynamic MassCom secondary electron multiplier and U was measured in static mode as U-oxide (assuming an ¹⁸O/¹⁶O composition of 0.00205 ± 0.000025) using Faraday cups fitted with 10¹³ Ω resistor amplifiers (von Quadt et al., 2016; Wotzlaw et al., 2017). The linearity of the MassCom secondary electron multiplier was calibrated through repeated measurements of SRM982 over a range of intensities. Instrumental mass bias fractionation was corrected for Pb and U by calculating the deviation of the measured ²⁰²Pb/²⁰⁵Pb and ²³³U/²³⁵U from the known tracer composition of the ET2535 tracer solution (Condon et al., 2015; McLean et al., 2015), respectively and the sample ²³⁸U/²³⁵U of 137.818 ± 0.045 (2σ; Heiss et al., 2012). Repeated analyses of total procedural blanks indicate that all of the analysed zircons contain no common Pb and all common Pb was introduced from the laboratory blank. All zircon measurements were corrected for common Pb using a laboratory blank composition of ²⁰⁶Pb/²⁰⁴Pb = 18.407 ± 0.197, ²⁰⁷Pb/²⁰⁴Pb = 15.191 ± 0.194 and ²⁰⁸Pb/²⁰⁴Pb = 36.926 ± 0.453, calculated through repeated total procedural blank measurements (n=18; uncertainties are 1σ). Data reduction and error propagation of the U-Pb data was carried out using Tripoli and U-Pb Redux software (Bowring et al., 2011) applying the algorithms of McLean et al. (2011) and the U decay constants of Jaffey et al. (1971). Uncertainties in the reported U-Pb dates are reported at a 95% confidence interval (2σ) and do not include decay constant uncertainties. All ²⁰⁶Pb/²³⁸U dates were corrected for initial ²³⁰Th disequilibrium (Schärer, 1984) using a variable Th/U_{melt}, by applying the experimentally determined D_{Th/U} = 0.25 ± 0.1 (Rubatto and Hermann, 2007).

References:

- Bowring, J., McLean, N. M., and Bowring, S., 2011, Engineering cyber infrastructure for U - Pb geochronology: Tripoli and U - Pb_Redux: *Geochemistry, Geophysics, Geosystems*, v. 12, no. 6, p. <http://dx.doi.org/10.1029/2010GC003479>.
- Condon, D., Schoene, B., McLean, N., Bowring, S., and Parrish, R., 2015, Metrology and traceability of U–Pb isotope dilution geochronology (EARTHTIME Tracer Calibration Part I): *Geochimica et Cosmochimica Acta*, v. 164, p. 464-480.
- Gerstenberger, H., and Haase, G., 1997, A highly effective emitter substance for mass spectrometric Pb isotope ratio determinations: *Chemical geology*, v. 136, no. 3, p. 309-312.
- Hiess, J., Condon, D. J., McLean, N., and Noble, S. R., 2012, $^{238}\text{U}/^{235}\text{U}$ systematics in terrestrial uranium-bearing minerals: *Science*, v. 335, no. 6076, p. 1610-1614.
- Jaffey, A., Flynn, K., Glendenin, L., Bentley, W., and Essling, A., 1971, Precision measurement of half-lives and specific activities of ^{235}U and ^{238}U *Physical Review C*, v. 4, no. 5, p. 1889-1906.
- Krogh, T., 1973, A low-contamination method for hydrothermal decomposition of zircon and extraction of U and Pb for isotopic age determinations: *Geochimica et cosmochimica acta*, v. 37, no. 3, p. 485-494.
- Márquez-Zavalía, M. F., and Heinrich, C. A., 2016, Fluid evolution in a volcanic-hosted epithermal carbonate–base metal–gold vein system: Alto de la Blenda, Farallón Negro, Argentina: *Mineralium Deposita*, v. 51, no. 7, p. 873-902.
- Mattinson, J. M., 2005, Zircon U–Pb chemical abrasion (“CA-TIMS”) method: combined annealing and multi-step partial dissolution analysis for improved precision and accuracy of zircon ages: *Chemical Geology*, v. 220, no. 1, p. 47-66.
- McLean, N. M., Bowring, J., and Bowring, S., 2011, An algorithm for U - Pb isotope dilution data reduction and uncertainty propagation: *Geochemistry, Geophysics, Geosystems*, v. 12, no. 6, p. <http://dx.doi.org/10.1029/2010GC003478>.
- McLean, N. M., Condon, D. J., Schoene, B., and Bowring, S. A., 2015, Evaluating uncertainties in the calibration of isotopic reference materials and multi-element isotopic tracers (EARTHTIME Tracer Calibration Part II): *Geochimica et Cosmochimica Acta*, v. 164, p. 481-501.
- Paton, C., Hellstrom, J., Paul, B., Woodhead, J., and Hergt, J., 2011, Iolite: Freeware for the visualisation and processing of mass spectrometric data: *Journal of Analytical Atomic Spectrometry*, v. 26, no. 12, p. 2508-2518.
- Rubatto, D., and Hermann, J., 2007, Experimental zircon/melt and zircon/garnet trace element partitioning and implications for the geochronology of crustal rocks: *Chemical Geology*, v. 241, no. 1, p. 38-61.
- Schärer, U., 1984, The effect of initial ^{230}Th disequilibrium on young U Pb ages: the Makalu case, Himalaya: *Earth and Planetary Science Letters*, v. 67, no. 2, p. 191-204.

von Quadt, A., Wotzlaw, J.-F., Buret, Y., Large, S. J., Peytcheva, I., and Trinquier, A., 2016, High-precision zircon U/Pb geochronology by ID-TIMS using new 10^{13} ohm resistors: Journal of Analytical Atomic Spectrometry, v. 31, p. 658-665.

Wotzlaw, J.-F., Buret, Y., Large, S.J., Szymanowski, D., von Quadt, A., 2017, ID-TIMS U-Pb geochronology at the 0.1‰ level using 10^{13} Ω resistors and simultaneous U and $^{18}\text{O}/^{16}\text{O}$ isotope ratio determination for accurate UO_2 interference correction: Journal of Analytical Atomic Spectrometry, v. 32, p. 579-586.

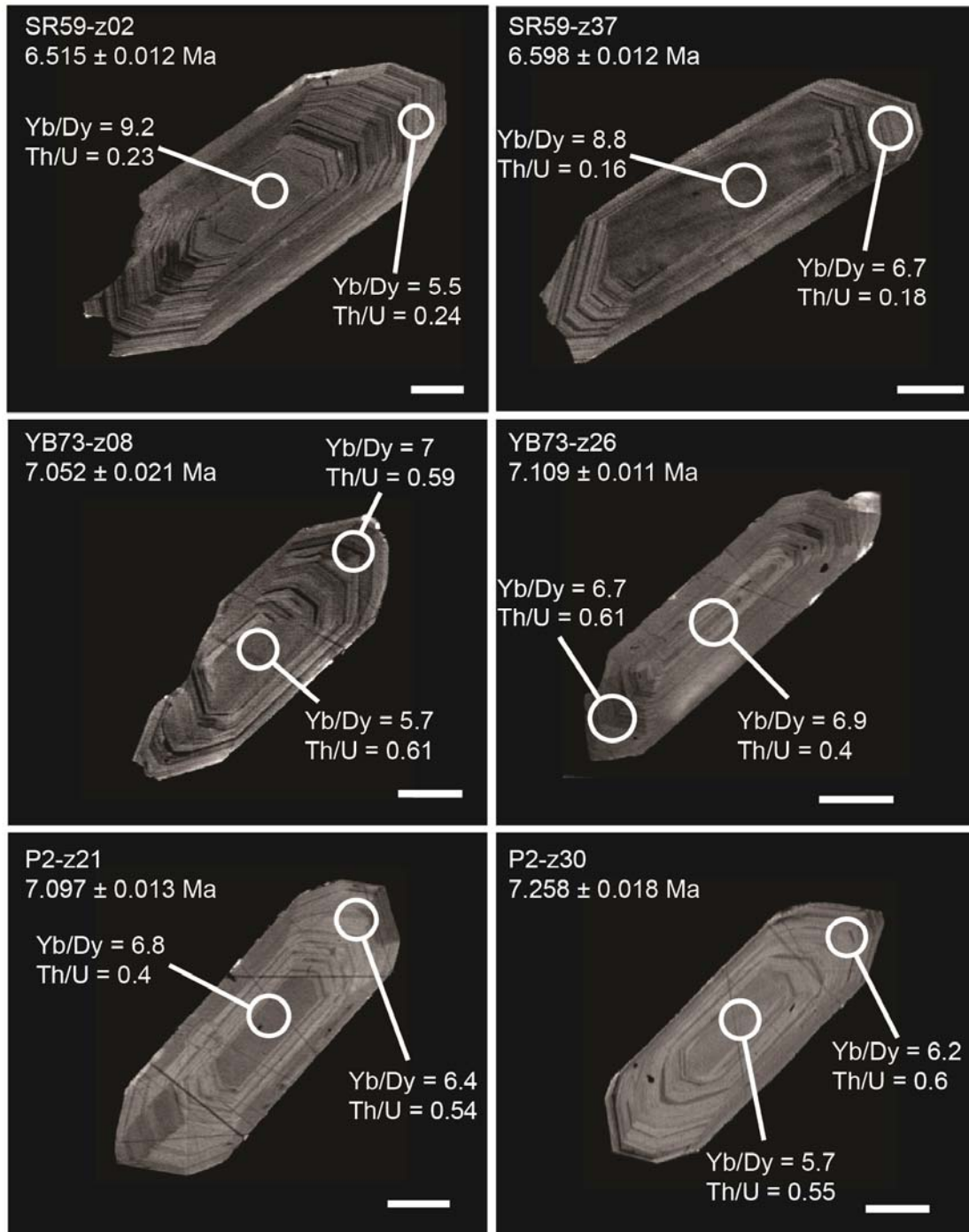


Fig. DR1. Representative cathodoluminescence images of zircons dated by CA-ID-TIMS showing locations of trace element analysis spots and corresponding trace element data. Scale bars = 50 μm .

Table DR1 and Table DR2

2017203_Tables DR1-DR2.xls